RSC Advances

ROYAL SOCIETY OF CHEMISTRY

www.rsc.org/advances

Synthesis and Characterization of High-Purity, Single Phase Hexagonal Bi_2Te_3 Nanostructures

L. Giri,[a*] G. Mallick,[a] A. C. Jackson,[b] M. H. Griep[a] and S. P. Karna[a]

Abstract

In order to synthesize defect free, highly crystalline single phase nanostructured bismuth chalcogenide, we have performed and analyzed the effects of several reaction conditions including, solvents, temperatures, reaction time, and reducing agents. A small variation in the reaction method resulted in Bi_2Te_3 with different morphologies, ranging from nanosize particles, rods, platelets, and tubes to nanosheets. The materials were characterized by powder X-ray crystallography, scanning electron microscopy, transmission electron microscopy, energy dispersive X-ray analysis, Raman spectroscopy, and four-probe current (I)-Voltage (V) analysis. An optimized reaction condition allowed the synthesis of single-phase, impurity-free hexagonal nanoplates with size varying between 50 nm and 500 nm and thickness varying between 45 nm and 55 nm in a reproducible manner. The Raman spectra of the optimized hexagonal plates and sheets showed infra red (IR)-active modes around 116 cm^{-1} resulting from symmetry breaking, a characteristic feature of nanostructured Bi_2Te_3. Additional peaks at 94 cm^{-1} in the nanosheets, resulting from the surface phonon mode further confirmed the ultrathin Bi_2Te_3 structures. The I-V measurements on the optimized surface showed an *n*-type semiconducting behavior. The surface current measured as a function of applied voltage is two orders of magnitude higher than that across the stacked pellet in ambient conditions and much higher compared to previously published data on few quintuplet-thick Bi_2Te_3 nanofilms. The highlights of this study are the optimal solvothermic reaction conditions and their impact on obtaining defect free, highly crystalline single phase bismuth chalcogenides.

Introduction

Bismuth telluride, Bi_2Te_3, among other chalcogenides, has been the subject of intense experimental and theoretical studies due to its excellent thermoelectric properties.[1-5] While the bulk Bi_2Te_3 has been extensively used in thermoelectric power generation devices, recent investigations have shown[6-9] that nanostructuring further enhances the thermoelectric figure of merit due to phonon scattering at nanodomains. In recent years, Bi_2Te_3 has also attracted attention as a three-dimensional topological insulator (TI),[10] whereby the bulk states possess regular gap in their band energy and the surface states exhibit electrical conduction due to the presence of mass less Dirac fermions.[11-14] Despite such novel properties and interest in Bi_2Te_3, there has been a lack of low-cost and scalable approach for reproducible synthesis of single-phase, impurity-free nano-structured Bi_2Te_3. Due to their simplicity and low cost, various wet chemistry methods, such as reverse micelle[15] and solvothermal synthesis in aqueous (hydrothermal)[16,17] as well as non-aqueous[18,19] media have been used recently to synthesize nanostructured Bi_2Te_3. Use of surfactants in solvothermal synthesis has been shown to result in extremely small particles of Bi_2Te_3.[20-23] Unfortunately, the solvothermal synthesis of Bi_2Te_3 is extremely sensitive to the reaction condition and even a small variation, such as the starting reactants, solvent, capping agent, temperature, and/or reaction time leads to nanostructured Bi_2Te_3 with widely varying morphology, size, structure, and impurity level in the materials.[24-28] In order to optimize reaction parameters for a scalable synthesis of defect-free bismuth telluride nanostructures with predicted and controlled morphology, we have efficiently studied the effects of reaction conditions including, solvents, reaction time, temperature, and reducing agent on solvothermal synthesis of Bi_2Te_3. We find that using bismuth chloride and tellurium powder as the starting material, a solvothermal synthesis in ethylene glycol medium with the use of polyvinylpyrrolidone (PVP having a molecular weight of 40,000) as surfactant and a reaction

time of 36 hours at 180˚C yields highly crystalline, single phase, 45-55 nm thick, hexagonal Bi_2Te_3 nanoplatelets with sizes varying from 50nm to 500 nm (distance between opposite sides of the hexagons). The high purity continuous phase of the nanoplatelets leads to a considerably large electrical current on the surface.

Experimental

Chemicals/materials. All the chemicals used in the present work were analytical grade obtained from Sigma Aldrich and used as received: bismuth chloride, ($BiCl_3$ with 97% purity), tellurium powder, (Te with 99.9% purity), sodium hydroxide (NaOH), sodium borohydride ($NaBH_4$ with 97% purity), polyvinylpyrrolidone (PVP) and ethylene glycol (EG).

The synthesis of Bi_xTe_y was carried out in two different media, namely (i) aqueous (A), and (ii) polyalcohol (P).

Synthesis of Bi_xTe_y in aqueous medium (AM). Four samples (AM-1 through AM-4) were obtained at different temperatures (100 – 180˚C) at fixed reaction time (12 h) and reducing agent ($NaBH_4$). 1.13 g (30 mmol) $NaBH_4$ and 0.96 g (7.5 mmol) tellurium were added into a flask containing 15 mL of 0.5 M NaOH. The reaction solution was heated approximately to 100˚ C and held for 15-20 min to complete the reaction till the formation of hydrogen was stopped (Equation 1). The solution turned into a pale purple color and then it was cooled naturally to room temperature. Next, 1.58 g (5 mmol) bismuth chloride was added in 15 mL deionized water and added in portions to the purple solution (Equation 2).

$$2NaBH_4(aq) + 5Te + 8NaOH \rightarrow 5Na_2Te + 3H_2(g) + 2B(OH)_3(aq) + 2H_2O \quad (1)$$

$$3Na_2Te + 2BiCl_3(aq) \rightarrow Bi_2Te_3 + 6NaCl \quad (2)$$

The reaction solution turned to a black suspension after heating to reflux for approximately 90 minutes. 10 mL of this black solution was taken and the precipitate was separated by centrifugation and washed with water, ethanol, and acetone and dried in vacuum at 60˚C for 2 hours. The next sample was prepared by augmenting the above procedure by hydrothermal treatment and adjusting the pH. The pH of the final black solution (10) was increased to 12 by adding a few drops of 0.5 M NaOH. The remaining black solution was now put into a 50 mL teflon-lined autoclave maintained at 120˚C for 12 h and then cooled to room temperature. The black precipitates were centrifuged and washed with distilled water, absolute ethanol and acetone in sequence. Finally, the dark products were dried in a vacuum at 60˚C for 2 h. Two additional samples were prepared by post synthesis treatment of the first sample with $NaBH_4$ and reacting for 12 h at 120˚C and 180˚C, respectively. The pH value was adjusted to 12.4 before the hydrothermal treatment. The final products were collected by centrifuging the black suspensions washed with water, ethanol and acetone and dried in vacuum at 60˚C for 2 hours. Table 1 summarizes the reaction parameters utilized.

Table 1. Sample Nomenclature

Sample	Solvent	Time (hours)	Temperature (˚C)	Reducing agent	M_w of PVP
AM-1	H_2O	12	100	$NaBH_4$	-
AM-2	H_2O	12	120	$NaBH_4$	-
AM-3	H_2O	12	120	$NaBH_4^*$	-
AM-4	H_2O	12	180	$NaBH_4^*$	-
PM-1	EG	12	180	EG	10,000
PM-2	EG	36	180	EG	10,000
PM-3	EG	12	180	EG	40,000
PM-4	EG	36	180	EG	40,000
*The samples AM-3 and AM-4 are post synthesized with $NaBH_4$					

Synthesis of Bi_xTe_y in polyol medium (PM). As in AM, four samples were prepared in PM with varying reaction parameters. Ethylene glycol (EG) with two different molecular weights (10,000 and 40,000) were used both as a solvent and a reducing agent. A total of 1 mmol (0.315 g) of $BiCl_3$, 1.5 mmol (0.19g) of Te, 0.4 g of NaOH, and 0.5 g of PVP (Mol. wt 10,000) were dissolved in 18 ml of EG, stirred with a magnetic stirrer for 30 minutes and then transferred into a stainless steel hydrothermal vessel (autoclave) with teflon liner . The autoclave was heated at 180˚C in an electric oven for 12 h and 36 h and then cooled naturally to room temperature. The black powder was collected by centrifuging, washed with distilled water, ethanol and acetone and finally dried at 60˚C in vacuum for 12 hours. The same synthesis process was applied for

another batch, but this time using a different polymer, PVP K-30 (Mol. wt 40,000). The nomenclatures of the samples are given in Table1.

To determine the electrical properties of bulk Bi_2Te_3, as prepared 50 mg of sample PM-4 was pressed under 1.5 GPa in a compressor to form a pellet.

Characterization The different crystal structures and corresponding phases in each sample were analyzed by powder X-ray diffraction (XRD) with a Rigaku-miniflex II diffractometer using Cu Kα radiation (λ = 1.541 Å). The phase identification and quantification (wt %) were carried out using MDI's Jade 8 software for all of the samples. The morphology of the products was analyzed by a Hitachi S4700 field emission scanning electron microscopy (FESEM) equipped with an energy-dispersive X-ray system (EDS) used for average compositional analysis. Transmission electron microscopy (TEM), high-resolution TEM (HRTEM), and selected area electron diffraction (SAED) of the nanostructures were observed on a JEOL JEM 2100F microscope at 200 kV using an Orius SC1000 camera. Raman spectra for nanostructured Bi_2Te_3 samples were recorded with a Horiba Jobin Yvon LabRam Aramis spectrometer at room temperature using a 532 nm excitation laser wavelength. The scattered light was analyzed with a spectrometer equipped with a detector. Both Raman and EDS results consist of an average of five measurements done at different locations on the samples. The electrical measurements were performed using Janis four-probe system and analyzed using Keithley 4200 semiconductor analyzer.

Results and Discussions Figure 1 presents typical FESEM images and XRD data of Bi_2Te_3 samples synthesized in aqueous medium for 12 hours at 100°C (Figure 1a), 120°C (Figure 1b and 1c), and 180°C (Figure 1d) using $NaBH_4$ as the reducing agent. Of note: Samples shown in Figure 1c and 1d were obtained after post synthesis treatment with $NaBH_4$of the first sample.

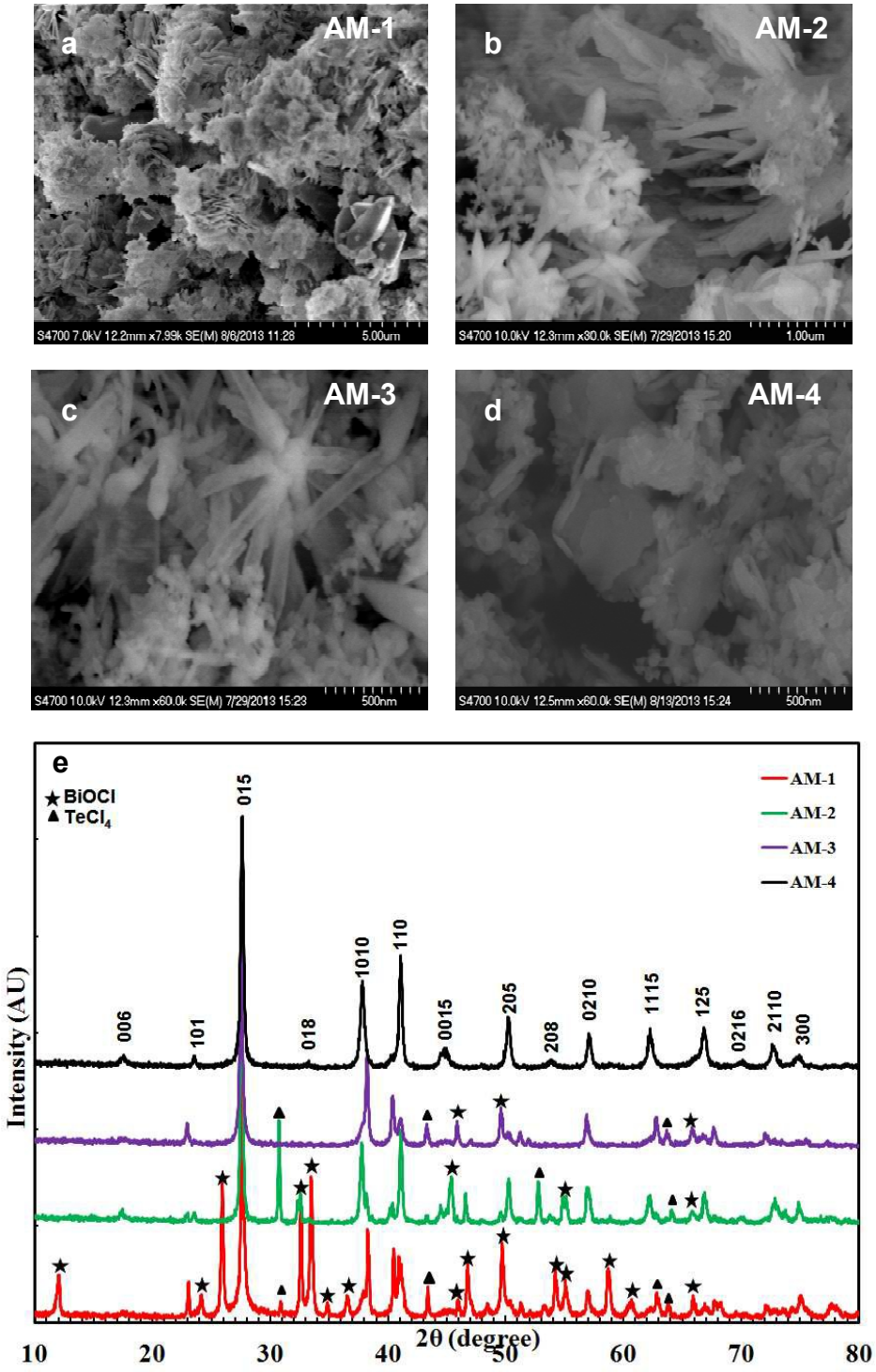

Figure 1. SEM images of as prepared Bi_2Te_3 in aqueous medium (AM) showing flower-like (a, b), nano-tubular (c), and 2D nanosheets (d). XRD patterns of the samples are shown in 2e.

As observed from the images the morphology varies greatly with change in synthesis parameters from flower-like (Figures 1a and 1b), nanotubular (Figure 1c) to two-dimensional nanosheets (Figure 1d). The samples obtained after the post synthesis treatment with $NaBH_4$ show more refined nanostructures as in Figures 1c and 1d. The EDS spectrum of these samples confirm the presence of Bi and Te. (Figure S2). The chemical composition and the crystalline phase structure of the as prepared Bi_2Te_3 nanostructures are shown in Figure 1e. Sample AM-1 has mainly peaks from BiOCl along with some characteristic lines of Bi_2Te_3 and $TeCl_4$. The Bi_2Te_3 lines get stronger with the modification of the synthesis condition, such as changing the reaction temperature, carrying out the reaction in a hydrothermal vessel and post synthesis treatment with $NaBH_4$. Sample AM-2 has prominent Bi_2Te_3 lines with fewer BiOCl. Sample AM-3 has mostly Bi_2Te_3 peaks with a couple of weak lines from BiOCl and $TeCl_4$. Finally, for sample AM-4, all peaks in the diffraction pattern correspond to the reflections of rhombohedral Bi_2Te_3. No detectable impurity peaks were observed, indicating that it has the rhombohedral lattice structure of Bi_2Te_3 (space group of $R\bar{3}m$).[27] The XRD pattern of the sample AM-4 has the characteristic features corresponding to (006), (101), (015), (018), (1010), (110), (0015), (205), (208), (0210), (1115),(125) ,(2110) and (300) planes according to the standard JCPDS card no.15-0863, The peaks labeled (015), (1010) and (110) are much stronger compared with other peaks in the x-ray pattern. The particle size of the sample AM-4 was estimated through the Debye – Scherrer equation, $d = k\lambda/\beta\cos\theta$, where k is 0.93, λ is CuKα wavelength (1.54 nm), β is the full width half maximum of the intense peak and θ is Bragg angle. The average crystallite size found is ~45 ± 10 nm.

The SEM images and corresponding XRD patterns of the samples prepared in polyol medium are shown in Figure 2. The morphology of samples PM-1 (Figure 2a) and PM-3 (Figure 2c), which

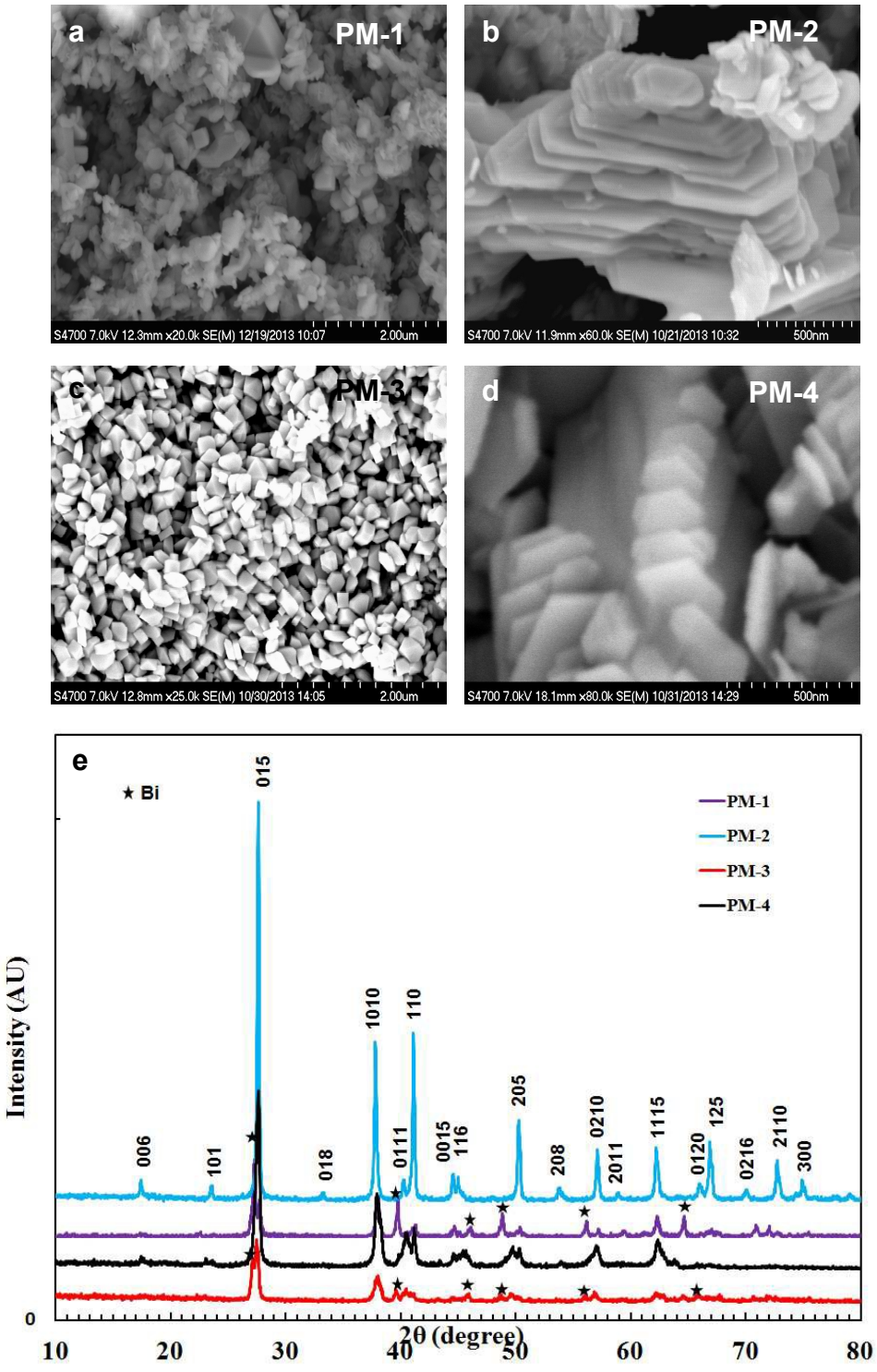

Figure 2. SEM images of as prepared Bi_2Te_3 in polyol medium (PM) showing rombohedron (a, c) and hexagonal platelet structures (b, d). XRD patterns of the samples are shown in 3e.

were obtained after 12 hours of reaction time with fixed temperature (180°C) and separate molecular weights (10,000 and 40,000) of reducing agents (EG), resembled regular rombohedron, with particle size varying between 50 nm and 200 nm. The sample PM-3 had well separated particles of uniform shapes and was prepared using PVP K-30 with higher molecular weight. Samples PM-3 and PM-4 were obtained after 36 hour reaction time at 180°C and 10,000 and 40,000 M.Wt of EG, respectively. The morphology changed to stacked hexagonal shaped plates (Figures 2b and 2d). The size of these nanoplates varied between 50 nm and 500 nm and the thickness varied between 50 nm and 60 nm. However, the hexagonal plates of PM-4 became thinner and separated (Figure 2d).

The XRD patterns of samples prepared in polyol medium are shown in Figure 3e. Samples PM-1 and PM-3, which were obtained after 12 hour reaction time, shows some peaks from Bi along with the Bi_2Te_3. Samples PM-2 and PM-4, obtained from 36 hour reaction time, show distinct peaks that can be indexed to the rhombohedral crystal system, (space group R3m), characteristic for Bi_2Te_3,[27] confirming the final product to be single phase Bi_2Te_3. Sample PM-2 (PVP 10,000 M.Wt., 36 hours) has the most intense and the sharpest XRD peaks from the synthesized Bi_2Te_3 nanocrystals, which are typical signatures of a high degree of crystallinity as confirmed by HRTEM. Compared to Figure 2, some higher order reflection from (0111), (2011), and (0120) planes are also present as confirmed from the standard literature value.[29] The calculated lattice constants, $a = b = 4.385$Å and $c = 30.487$ Å are in very good agreement with the standard literature values ($a = b = 4.385$ Å and $c = 30.483$ Å; JCPDF #15-0863). The average estimated particle size for sample PM-2 i ~40 ± 10 nm. The particles in samples PM-3 and PM-4 got smaller compared to those in PM-1 and PM-2 (Figure 2e).

Since, samples AM-4 and PM-4 were mostly free of impurities we determined to investigate them further. The fine microstructure of the Bi_2Te_3 nanotubes and nanoprticles were also studied by transmission electron microscopy (TEM) and high-resolution TEM (HRTEM).

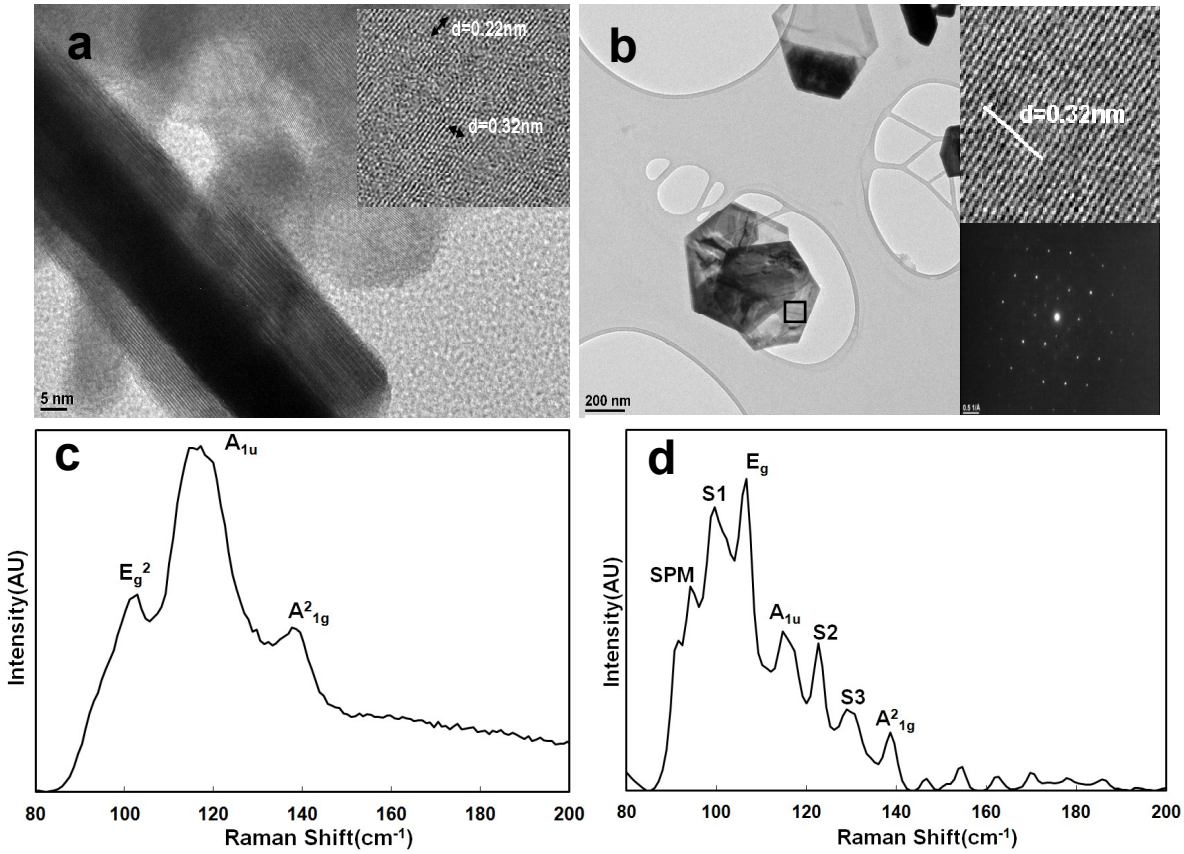

Figure 3. HRTEM images with their respective lattice spacing (insets) of AM-4 (a) and PM-4 (b). The lower inset of 3(b) shows the SAED of PM-4. The corresponding Raman spectra from AM-4 and PM-4 in (c and d), respectively.

The TEM images of sample AM-4 (Figure 3 (a)) (also see Figure S1 in the supporting information) show irregularly shaped nanoparticles including nanorods. The HRTEM image of AM-4 in Figure 3a show structurally uniform the lattice fringes, with a spacing of 0.22 nm and 0.32 nm, in good agreement with the *d* value of the (110) and (015) planes, respectively, of rhombohedral Bi_2Te_3 according to the standard JCPDS card no.15-0863.

Sample PM-4, prepared in the polyol medium, consisted of uniformly distributed hexagonal nanoplates as seen from the TEM images (also see Figure S3). The size of these nanoplates, measured between the opposite sides of the hexagons, varied from 50 nm to 500 nm. The thickness of a single nanoplate, measured by electron energy loss spectroscopy (EELS), varied between 45 nm and 55 nm. The high contrast (dark over transparent crystals) areas in the TEM images (Figure 3 (b), Figure S3) are evidence of the ultrathin nature of the nanocrystals.

The nanosheets exhibit a high degree of crystallinity, evidenced by flat surface and sharp edges. Ripple-like contrasts observed in some crystal surfaces most probably result from surface strain and/or non-uniformity in thickness, as also reported earlier.[25]

The HRTEM images were taken from the marked area of Figure 3b. The lattice shown in the HRTEM image (upper inset of Figure 3b) and the spot pattern of SAED (lower inset of Figure 3b) demonstrate the crystalline nature of the nanoplate. The lattice fringes were structurally uniform with a spacing of 0.32 nm, which is in good agreement with the *d*-spacing of the (015) planes of rhombohedral Bi_2Te_3 (JCPDS card no.15-0863). The SAED pattern taken from a single nanoplate confirms the hexagonal symmetry of the crystal plane. The bright diffraction spots are indicative of the high degree of crystallinity and also suggest the absence of planar structural defects. The *d* spacings calculated from the diffraction spots match with those obtained from PXRD pattern. The EDS spectrum of sample PM-4 (Figure S2) taken from the same marked area as in Figure 3b show the presence of elemental bismuth and tellurium alone, confirming the purity of the final product. The Cu lines appearing in the spectrum are due to the copper grids of the sample holder.

The local atomic arrangements and the nature of chemical bonds in the synthesized nanosheets (sample AM-4) and nanoplates (sample PM-4) were also investigated by Raman spectroscopy (Figure 3c and 3d). The Raman spectrum of bulk crystalline Bi_2Te_3 is known to exhibit three active modes, namely A^1_{1g} at 61 cm^{-1}, E^2_g at 102 cm^{-1}, and A^2_{1g} at 134 cm^{-1}.[30] The states labeled "E" and "A" indicated the in-plane and out-of-plane lattice vibrations, respectively. The subscript "g" (*gerade* for symmetric) denotes Raman-active, while "u" (*ungerade* for asymmetric) represents Raman-inactive but IR-active modes. In addition to the classical Raman-active modes, both samples show an additional peak between around 118 cm^{-1} which could be ascribed to the A^1_u mode.[26,31-36] Bi_2Te_3 is centro-symmetric and therefore A^1_u mode is Raman forbidden. However, for the nanostructured samples low dimensional structure breaks down the centro-symmetric nature of the bulk Bi_2Te_3 and A^1_u peaks appear in Raman spectrum[26,31-36]. For the hexagonal nanoplates (sample PM-4), additional vibration modes also show up. The peak at 94 cm^{-1} results from the surface phonon mode (SPM), only observed in nano-sized materials and the peak S2 is an infrared-active mode due to the size effect.[35] The origin of peaks labeled S1 and S3 could not be identified and needs further study to categorize them to defects in nanostructures.

To understand the electrical properties of the synthesized Bi_2Te_3 nanoplatlets, several measurements of current (I) with respect to drain voltage (V) were performed on the surface and across the carefully prepared pellet of Bi_2Te_3 at room temperature. Figure 4 shows the I-V characteristics of the as prepared Bi_2Te_3 pellet probed by a semiconductor (SC) analyzer (Keithley-4200) attached to a four-probe micromanipulater system (Janis) at high (+/-3V) (Figure 4a) and low (+/-0.5V) (Figure 4b) source - drain voltage sweeps. The inset of Figure 4b

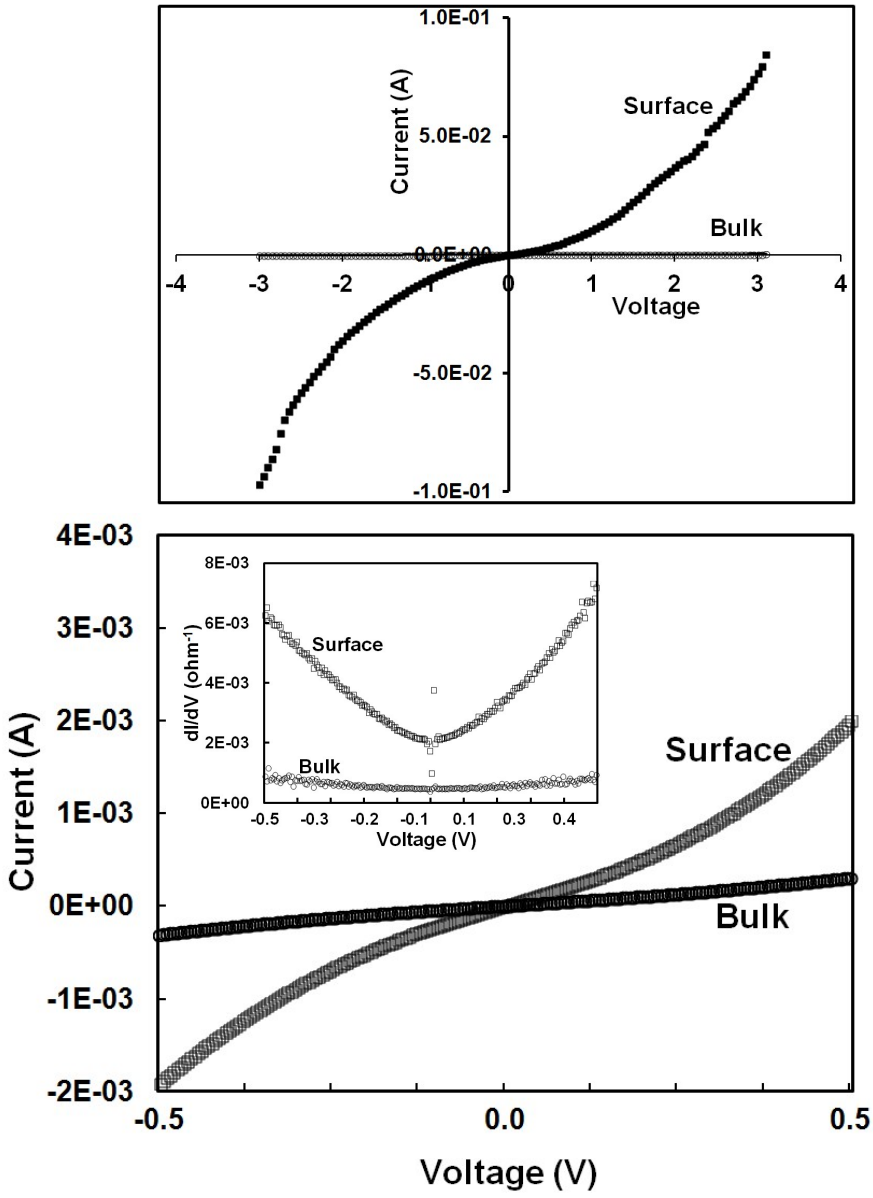

Figure 4. Current (I) – Voltage (V) measurements of Bi_2Te_3 pellet surface (square) and bulk (circle) at high (a) and low (b) voltages. The conductance (inset) of the I-V is shown in 4b.

is the conductance (dI/dV) plot at low drain voltage. The I-V characteristics of the Bi_2Te_3 nanoplatlets surface show an *n*-type semiconducting behavior, with a distinct non-linearity for higher voltage sweep, qualitatively similar to that recently reported by Teweldebrhan et al.,[36] but showing a rather much higher current, which shows a high purity, defect free single phase

crystalline surface of the synthesized nanoplatlets. With the bottom of the pellet contacted to a metal (steel) gate, no gating effect was noticed even at a high gate potential of +/-20V, similar to that observed for a few quintuple-thick film samples previously reported. [36] In the present case, this could result from a rather rough interface and loose packing between the nanostructured pellets. This is confirmed by a negligible current across the 0.5 mm pellet as shown in Figure 4 for high and low voltage sweeps. High electrical current at the surface of the nanostructured pellets would be advantageous for electronic devices as well as for investigating quantum mechanical effects.

Conclusion

In summary, we have investigated the effect of reaction parameters on the morphology, structure, purity, and crystallinity of nanostructured Bi_2Te_3 materials. Careful optimization of the reaction parameters allowed a successful synthesis of highly pure Bi_2Te_3 nanostructures with different morphologies, depending on the synthesis conditions. While the morphology of the samples prepared in the aqueous medium varied significantly with the reaction parameters, those prepared in the polyol medium had mostly hexagonal nanoplates. We find that a reaction time of 36 hours and PVP, with molecular weight of 40,000, as the surfactant yield a highly crystalline, single phase hexagonal shaped Bi_2Te_3 nanoplates of 50-500 nm size and 45-55 nm thickness. The presence of the infrared (IR) active mode (A_{1u}), in the Raman spectrum confirms the symmetry breaking in ultra-thin Bi_2Te_3 nanosheets and hexagonal nanoplates. The as-synthesized hexagonal nanoplates, showing unique Raman optical properties compared to bulk crystals, may find novel applications in thermoelectric and spin-Hall devices. The high surface

electrical conductance of the nanoplates also suggests potential applications in two-dimensional electronics applications.

Acknowledgements

This research by one of us (L. G.) was supported in part by an appointment to the Research Participation Program at the U.S. Army Research Laboratory (US ARL) administered by the Oak Ridge Institute for Science and Education through an inter agency agreement between the U.S. Department of Energy and US ARL. Fruitful discussions with Kate Duncan are gratefully acknowledged.

Electronic Supplementary Information (ESI) available: Additional TEM and EDS data on synthesized samples supplied as Supporting Information are available at http://pubs.esc.org.

Notes
[a] US Army Research laboratory, WMRD, Aberdeen Proving Ground, MD-21005
[b] Axalta Coating Systems, Wilmington, DE 19803
[*]Oakridge Institute of Science and Education (ORISE) Senior Associate

References

1. G. J. Snyder and E. S. Toberer, *Nat Mater*, 2008, **7**, 105-114.
2. J. R. Sootsman, D. Y. Chung and M. G. Kanatzidis, *Ang. Chemie Intl. Ed.*, 2009, **48**, 8616-8639.
3. L. E. Bell, *Science*, 2008, **321**, 1457-1461.

4. B. Poudel, Q. Hao, Y. Ma, Y. Lan, A. Minnich, B. Yu, X. Yan, D. Wang, A. Muto, D. Vashaee, X. Chen, J. Liu, M. S. Dresselhaus, G. Chen, and Z. Ren, *Science*, 2008, **320**, 634-638.
5. W. Kim, J. Zide, A. Gossard, D. Klenov, S. Stemmer, A. Shakouri, and A. Majumdar, *Phys. Rev. Lett.*, 2006, **96**, 045901.
6. S. K. Bux, R. G. Blair, P. K. Gogna, H. Lee, G. Chen, M. S. Dresselhaus, R. B. Kaner, and J.-P. Fleurial, *Adv. Func. Mat.*, 2009, **19**, 2445-2452.
7. J. R. Szczech, J. M. Higgins, and S. Jin, *J. Mat. Chem.*, 2011, **21**, 4037-4055.
8. M. S. Dresselhaus, G. Chen, M. Y. Tang, R. G. Yang, H. Lee, D. Z. Wang, Z. F. Ren, J. P. Fleurial, and P. Gogna, *Adv. Mat.*, 2007, **19**, 1043-1053.
9. M. G. Kanatzidis, *Chem. Mat.*, 2009, **22**, 648-659.
10. D. Hsieh, Y. Xia, D. Qian, L. Wray, F. Meier, J. H. Dil, J. Osterwalder, L. Patthey, A. V. Fedorov, H. Lin, A. Bansil, D. Grauer, Y. S. Hor, R. J. Cava, and M. Z. Hasan, *Phys. Rev. Lett.*, 2009, **103**, 146401.
11. R. Yu, W. Zhang, H.-J. Zhang, S.-C. Zhang, X. Dai, and Z. Fang, *Science*, 2010, **329**, 61-64.
12. J. Moore, *Nat. Phys*., 2009, **5**, 378-380.
13. D. Kong, and Y. Cui, *Nat Chem*., 2011, **3**, 845-849.
14. C. L. Kane, and E. J. Mele, *Phys. Rev. Lett.*, 2005, **95**, 146802.
15. E. E. Foos, R. M. Stroud, and A. D. Berry, *Nano Lett.*, 2001, **1**, 693-695.
16. R. O. Jyoti, R. Poulomi, K. S. Suneel, R. Popovitz-Biro, and T. Reshef, *Nanotechnology*, 2006, **17**, 1700-1705.

17. M. Salavati-Niasari, M. Bazarganipour, and F. Davar, *J. Alloys and Compds.*, 2010, **489**, 530-534.

18. G. Zhang, W. Wang, X. Lu, and X. Li, *Cryst. Growth and Design*, 2008, **9**, 145-150.

19. Y. Liang, W. Wang, B. Zeng, G. Zhang, Q. He, and J. Fu, *Mat. Chem. and Phys.*, 2011, **129**, 90-98.

20. N. Mntungwa, P. V. S. R. Rajasekhar, K. Ramasamy, and N. Revaprasadu, *Superlattices and Microstructures*, 2014, **69**, 226-230.

21. M. R. Dirmyer, J. Martin, G. S. Nolas, A. Sen, and J. V. Badding, *Small*, 2009, **5**, 933-937.

22. M. Scheele, N. Oeschler, K. Meier, A. Kornowski, C. Klinke, and H. Weller, *Adv. Funct. Mat.*, 2009, **19**, 3476-3483.

23. A. Purkayastha, A. Jain, C. Hapenciuc, R. Buckley, B. Singh, C. Karthik, R. J. Mehta, T. Borca-Tasciuc, and G. Ramanath, *Chem. Mat.*, 2011, **23**, 3029-3031.

24. U. Pelz, K. Kaspar, S. Schmidt, M. Dold, M. Jägle, A. Pfaadt, and H. Hillebrecht, *J. Elec. Mat.*, 2012, **41**, 1851-1857.

25. Y. Zhang, L. P. Hu, T. J. Zhu, J. Xie, and X. B. Zhao, *Cryst. Growth and Design*, 2013, **13**, 645-651.

26. G. D. Keskar, R. Podila, L. Zhang, A. M. Rao, and L. D. Pfefferle, *J. Phys. Chem. C*, 2013, **117**, 9446-9455.

27. Y. Feutelais, B. Legendre, N. Rodier, and V. Agafonov, *Mat. Res. Bulletin*, 1993, **28**, 591-596.

28. S. Derrouiche, C. Z. Loebick, and L. Pfefferle, *J. Phy. Chem. C*, 2010, **114**, 3431-3440.

29. H. E. Swanson, M. C. Morris, and E. H. Evans, *Nat. Bur. of Standards Monograph*, 1966, **28**, 21-22.

30. V. Russo, A. Bailini, M. Zamboni, M. Passoni, C. Conti, C. S. Casari, A. Li Bassi, and C. E. Bottani, *J. Raman Spect.*, 2008, **39**, 205-210.

31. K. M. F. Shahil, M. Z. Hossain, V. Goyal, and A. A. Balandin, *J. Appl. Phys.*, 2012, **111**, 054305.

32. S. M. Souza, D. M. Triches, C. M. Poffo, J. C. deLima, T. A. Grandi, and R. S. de Biasi, *J. Appl. Phys.*, 2011, **109**, 1-8.

33. Y. Zhao, R. W. Hughes, Z. Su, W. Zhou, and D. H. Gregory, *Angew. Chem., Int.* Ed., 2011, **50**, 10397-10401.

34. Y. Liang, W. Wang, B. Zeng, G. Zhang, J. Huang, J. Li, T. Li, Y. Song, and X. Zhang, *J. Alloys and Compounds*, 2011, **509**, 5147-5151.

35. C. Wang, X. Zhu, L. Nilsson, J. Wen, G. Wang, X. Shan, Q. Zhang, S. Zhang, J. Jia, and Q. Xue, *Nano Res.*, 2013, **6**, 688-692.

36. D. Teweldebrhan, V. Goyal, and A. A. Balandin, *Nano Lett.*, 2010, **10**, 1209-1218.

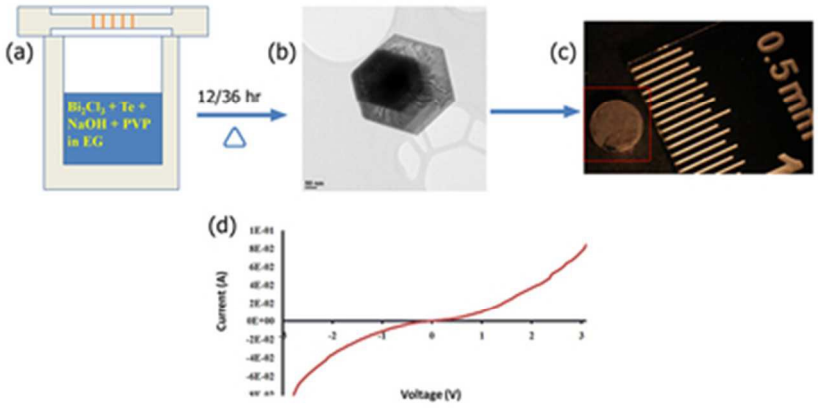

Schematic solvothermal synthesis of Bi_2Te_3 (a) producing bulk Bi_2Te_3 (SEM image - b) which was converted into pellet (c). The electrical characterization (d) of the Bi_2Te_3 pellet surface showed significantly high current (100 folds) than the bulk.
36x17mm (300 x 300 DPI)